CHEMISTRY
A EUROPEAN JOURNAL

DOI: 10.1002/chem.201001908

Vapochromic and Mechanochromic Tetrahedral Gold(I) Complexes Based on the 1,2-Bis(diphenylphosphino)benzene Ligand

Masahisa Osawa,*[a, b] Isao Kawata,[a] Satoshi Igawa,[a] Mikio Hoshino,[a] Takeo Fukunaga,[c] and Daisuke Hashizume[c]

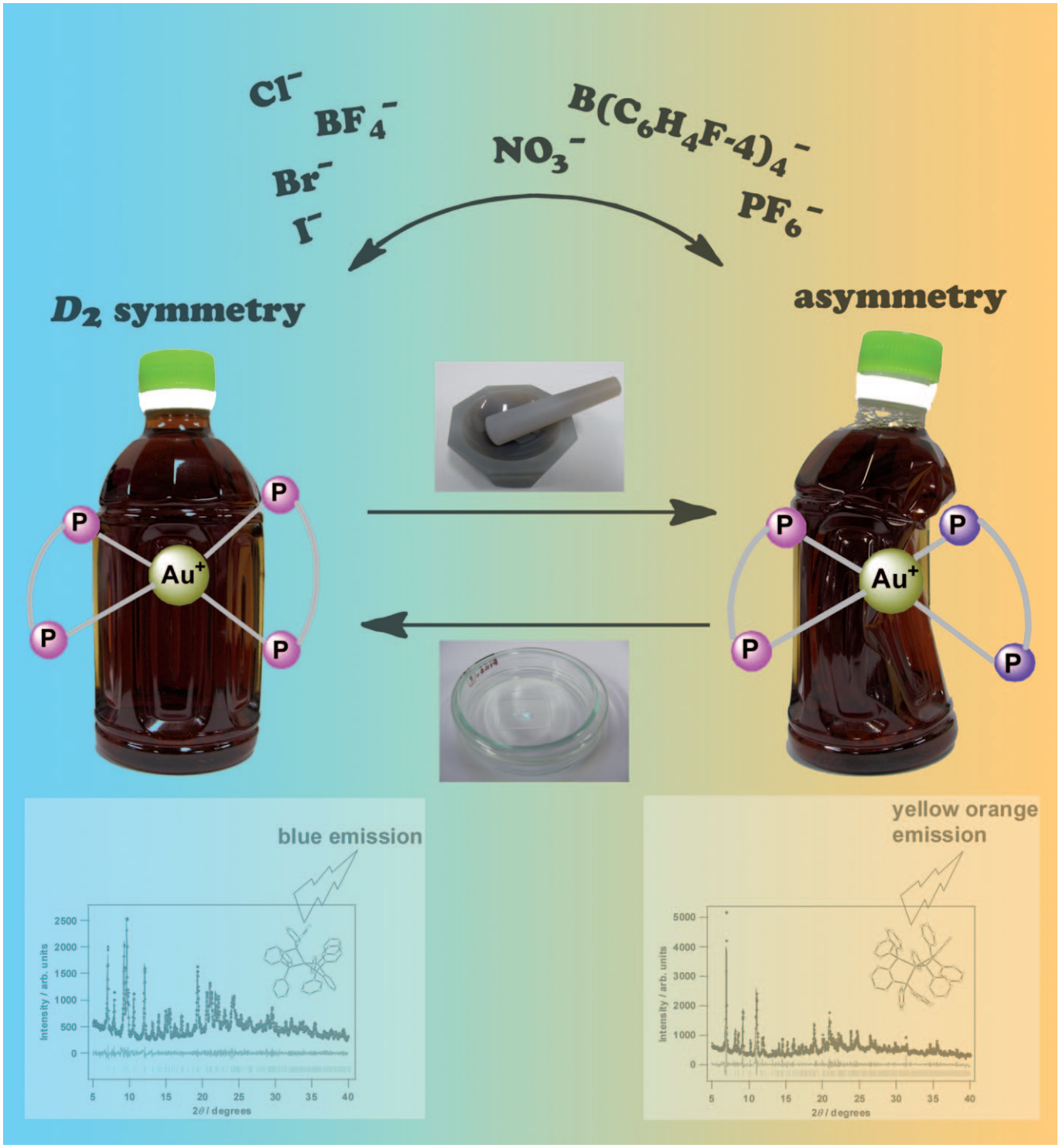

Abstract: Tetrahedral gold(I) complexes containing the diphosphane ligand (dppb = 1,2-bis(diphenylphosphino)benzene), $[Au(dppb)_2]X$ [X = Cl (**1**), Br (**2**), I (**3**), NO_3 (**4**), BF_4 (**5**), PF_6 (**6**), $B(C_6H_4F\text{-}4)_4$ (**7**)], and the ethanol and methanol adducts of complex **4**, **8**, and **9**, were prepared to analyze their unique photophysical properties. These complexes are classified into two categories on the basis of their crystal structures. In Category I, the complexes (**1**–**5**) have relatively-small counter anions and two dppb ligands are symmetrically coordinated to the central Au^I atom, and display an intense blue phosphorescence. Alternatively, the complexes (**6**–**9**) in Category II have large counter anions and two dppb ligands asymmetrically coordinated to Au^I atom, and display a yellow or yellow orange phosphorescence. The difference in the phosphorescence color of the complexes between the Category I and II is ascribed to the change in the structure of the cationic moiety in the complex. According to DFT calculations, the symmetry reduction caused by the large counter anion of the complex in Category II gives the destabilization of HOMO (σ*) levels, leading to the red-shift of the emission peak. We have demonstrated that the symmetry reductions are responsible for the phosphorescence color alteration caused by external stimuli (volatile organic compounds and mechanical grinding).

Keywords: density functional calculations · gold · ligand effects · mechanochromism · phosphorescence · vapochromism

Introduction

Luminescent materials are widely applicable for molecular imaging and sensors of chemicals and biological molecules, because of their quick response, high sensitivity, and facile visual detection of luminescence.[1,2] Among them, the development of solid chemical sensors based on luminous metal complexes with high stability has received increasing attention. Some examples are sensors for volatile organic compounds (VOCs).[3–37] Furthermore, a new concept of sensing motion and changes in mechanical force has recently been proposed, luminescence mechanochromism and tribochromism.[38–47] Vapo- and mechanoluminescent complexes in the solid state show reversible emission-color changes in the visible or near-infrared regions. These spectral shifts, as responses of VOCs or mechanical force, generally originate from molecular conformation changes in the solid state, e.g., metal–metal distance,[3–22,40,41,43–45] coordination of VOCs,[23–26] trapped VOCs in a crystal lattice,[27–29] weak noncovalent interactions (π–π interaction, hydrogen bonding, CH–π interactions),[8,11,19,20,26,30–36,40,43,47] isomerization involving polymer complexes and oligomers,[37] and planarization of the conjugated ligand.[46] Up to now, a number of linearly-coordinated Au^I systems have been reported as vapoluminescent compounds[3,6,9] or mechanoluminescent materials.[39–41,43,44] In these complexes two coordinated Au^I complexes aggregate through intermolecular aurophilic interactions,[48–50] causing the structural changes responsible for alterations of their luminescence color.

We have previously reported phosphorescence color alterations by changing the counter anions in crystals in tetrahedral gold(I) complexes $[Au(dppb)_2]X$ [dppb = 1,2-bis(diphenylphosphino)benzene)] (X = Cl, BF_4 and PF_6) (Scheme 1).[51] The symmetrical coordination of two dppb ligands to the Au atom seems to be necessary for the intense blue phosphorescence from tetrahedral gold(I) complexes (X = Cl, BF_4). A small conformational change of the two dppb ligands in the crystalline state caused by changing the counter anions dramatically alters the phosphorescence color from blue to yellow orange.

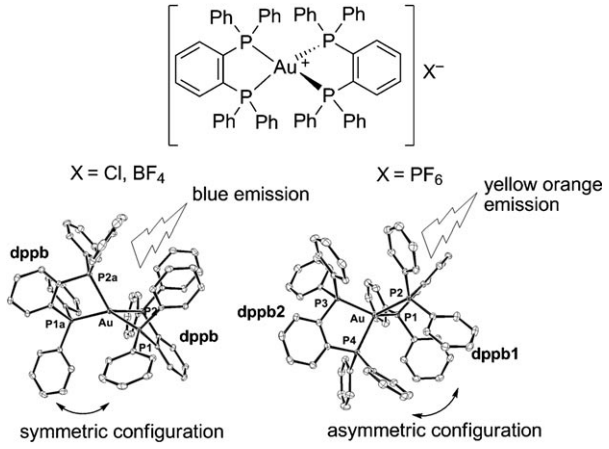

Scheme 1. Structures of $[Au(dppb)_2]^+$ and phosphorescence color.

[a] Dr. M. Osawa, Dr. I. Kawata, S. Igawa, Dr. M. Hoshino
Luminescent Materials Laboratory
RIKEN (The Institute of Physical & Chemical Research)
Hirosawa 2-1, Wako-Shi, 351-0198 (Japan)
Fax: (+81) 48-462-1767
E-mail: osawa@postman.riken.jp

[b] Dr. M. Osawa
Supramolecular Science Laboratory
RIKEN (The Institute of Physical & Chemical Research)
Hirosawa 2-1, Wako-Shi, 351-0198 (Japan)

[c] Dr. T. Fukunaga, Dr. D. Hashizume
Advanced Technology Support Division
RIKEN (The Institute of Physical & Chemical Research)
Hirosawa 2-1, Wako-Shi, 351-0198 (Japan)

Supporting information for this article is available on the WWW under http://dx.doi.org/10.1002/chem.201001908.

In this work, luminescence studies have been carried out for the Au^I complexes with a series of counter anions to have a better understanding on the phosphorescence color alteration in the solid state. The structures and photophysical properties of dppb and mononuclear tetrahedral Au^I complexes have been studied, $[Au(dppb)_2]X$ [X = Cl (**1**), Br (**2**), I (**3**), NO_3 (**4**), BF_4 (**5**), PF_6 (**6**), $B(C_6H_4F\text{-}4)_4$(**7**)], including a selective and reversible vapochromic response of complex **4** and the mechanochromic properties of complexes **1**–**9**. The differences in the absorption and emission spectra between **1**–**5** and **6**–**9** [**4**·2 EtOH (**8**), **4**·3 MeOH (**9**)], have been interpreted on the basis of molecular arrangement including packing structures of the complexes and time-dependent density functional theory (TD DFT) calculations.

Results and Discussion

Photophysical properties of dppb in the solid state: The dppb ligand has two types of aromatic groups attached to P atoms: one is the bridging *o*-phenylene group and the other, the phenyl group. Solutions of dppb are not emissive at room temperature,[52] but the weak blue emission centered at $\lambda = 477$ nm is observed in the solid state, as shown in Figure 1b.[51] The emission quantum yield (Φ) is obtained as

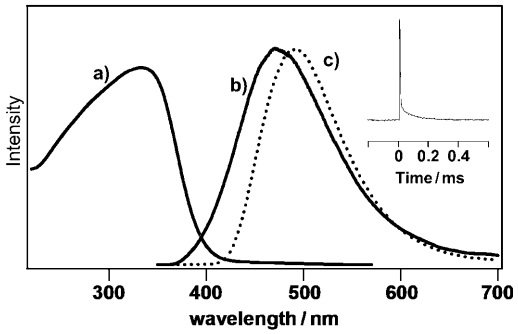

Figure 1. Absorption and corrected emission spectra of dppb in the crystalline state; absorption spectrum a) at 293 K, and emission spectra, b) at 293 K, and c) at 77 K ($\lambda_{exc} = 350$ nm). The inset shows the decay profile of emission observed for dppb after $\lambda = 355$ nm laser pulse at 293 K.

0.02. The absorption spectrum (Figure 1a) in the solid state exhibits an intense UV band, characteristic of arylphosphine, centered at about $\lambda = 350$ nm, which is attributed to a $l \rightarrow \pi^*$ transition of $n \rightarrow \pi^*$ character.[53,54] This type of transition involves the promotion of an electron from the lone pair orbital (l) on the phosphorus atom to an empty antibonding π orbital, π^*, of a phenyl group attached to the P atom.

The assignment of the $l \rightarrow \pi^*$ transition is also supported by the DFT calculations. According to the calculations, of the emitting states of dppb, the CT state from the lone pair on the phosphorous atom to the bridging phenylene group contributes the most, and thus, the hole (approximately HOMO) of dppb locates on the P atom, and the electron (approximately LUMO) is largely confined to the bridging *o*-phenylene group (Figure 2, S_1/a and S_1/b). The decay of the weak blue emission at room temperature is composed of

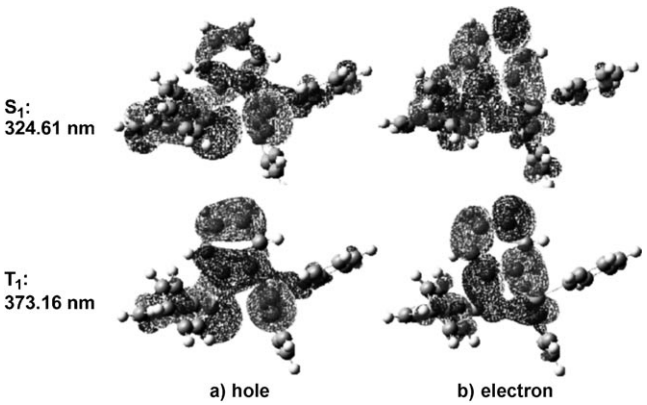

Figure 2. Natural transition orbital pairs for the S_1 and T_1 of dppb; a) hole, b) electron.

two components: the lifetime of the faster decay component (fluorescence) is < 20 ns and the slower one 77 μs, as represented in the inset in Figure 1. An anomalous long-lived emission from dppb at room temperature is assumed to be E-type delayed fluorescence. The following observations support this assumption: 1) at 77 K, the emission peak maximum in the solid state slightly shifts to red from $\lambda = 477$ to 490 nm and the lowest excited singlet and triplet energy difference estimated from these emission spectra is only 5–7 kcal mol^{-1} (Figure 1b,c), 2) the lifetime at 77 K becomes as long as 12 ms, and 3) the emission quantum yield increases up to 0.90 at 77 K. The thermally activated delayed fluorescence has frequently been observed if the singlet–triplet (S–T) energy gap is small, and thus, a thermal equilibrium is attained between singlet and triplet states. The small S–T energy gap for dppb is further substantiated by the DFT calculation results. As shown in Figure 2, the S_1–T_1 energy difference is 11.5 kcal mol^{-1} and the maps of the hole and the electron are very similar between S_1 and T_1.

Synthesis and structural characterization of tetrahedral gold(I) complexes: To a tetrahydrofuran solution of $[Au(PPh_3)]Cl$ was slowly added dppb powder. After standing still for 20 min, white precipitates of $[Au(dppb)_2]Cl$ (**1**) were obtained almost quantitatively. The other Au^I complexes were synthesized in high yield by exchanging the counter anion of complex **1**. The nine different single crystals with seven different counter anions were obtained by recrystallization from various solvents. Complexes **8** and **9** are the ethanol and the methanol adducts of complex **4**, respectively. The molecular structures of these complexes were determined by X-ray diffraction analysis. These crystal structures are classified into two categories on the basis of their struc-

tural features. The crystallographic data and the results of the structure refinements are summarized in Tables S1 and S2 (Categories I and II, respectively) in the Supporting Information. The complexes in Category I have two dppb ligands symmetrically coordinated to the Au^{I} atom in the cationic molecule, and thus the space group is *P*2/*n*. Complexes **1**–**5** belong to this category and have very similar crystallographic parameters (see Table S1 in the Supporting Information). The ORTEP drawing of $[Au(dppb)_2]NO_3$ (**4**) is shown in Figure 3 as a representative example of this category, and structures of **1**–**3** and **5** are shown in Figures S1–S5. The bond lengths and angles of **1**–**5** are shown in Tables S3 and S4. The Au atoms in **1**–**5** are in a highly distorted tetrahedral coordination geometry with a dihedral angle of 84.08–87.19° between the planes defined by P1-Au-P2 and P1a-AuP-2a. Because of the short distance (3.770–3.844 Å) between the centroids of the adjacent two phenyl groups in the dppb ligands of complexes **1**–**5**, we consider that there exists an intraligand π–π interaction between a nonbridging phenyl group on P(1) and another on P(2) in each dppb ligand (Figure 3), and that these interligand π–π interactions in the dppb ligands are necessary for supporting the symmetrical coordination geometry of the cationic molecule in complexes **1**–**5**. In contrast to the complexes in Category I, those in Category II have two asymmetric dppb ligands coordinated to the Au^{I} atom to give a tetrahedral geometry that is more distorted than the complexes in Category I. The dihedral angle (77.06–82.33°) between the two planes, P1-Au-P2 and P3-Au-P4, bond lengths and angles of **6**–**9** are listed in Tables S5 and S6 in the Supporting Information. Complexes **6**–**9** reside in this category and their molecular structures are shown in Figure 4. Although no intraligand π–π interaction of phenyl groups can be seen, we assume that there are one or two weak interligand π–π interactions between nonbridging phenyl groups in **6**–**9** (the distance between the centroid of two phenyl groups is 3.873–4.147 Å).

In Category I, all intermolecular interactions symmetrically work on each ligand because of the equivalence of the two dppb ligands in crystals. Conversely, in Category II, intermolecular interactions are asymmetric. The weak noncovalent intermolecular interactions (CH/π[55], CH/O[56,57], CH/F[58–60] interactions) in single crystals of **4**–**9** are summarized in Tables S7–S11 in the Supporting Information. If a counter anion is small, the anion fits in

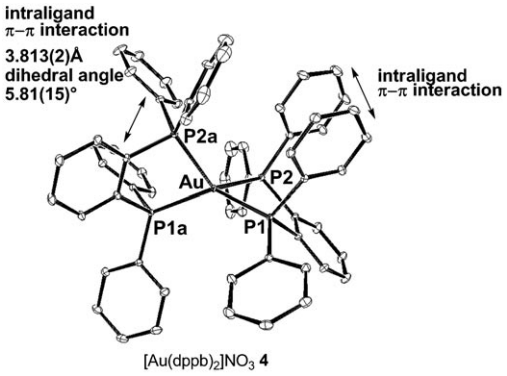

Figure 3. Molecular structure of **4** in Category I. Thermal ellipsoids are drawn at 50% probability level. Hydrogen atoms and counter anion NO_3^- omitted for clarity.

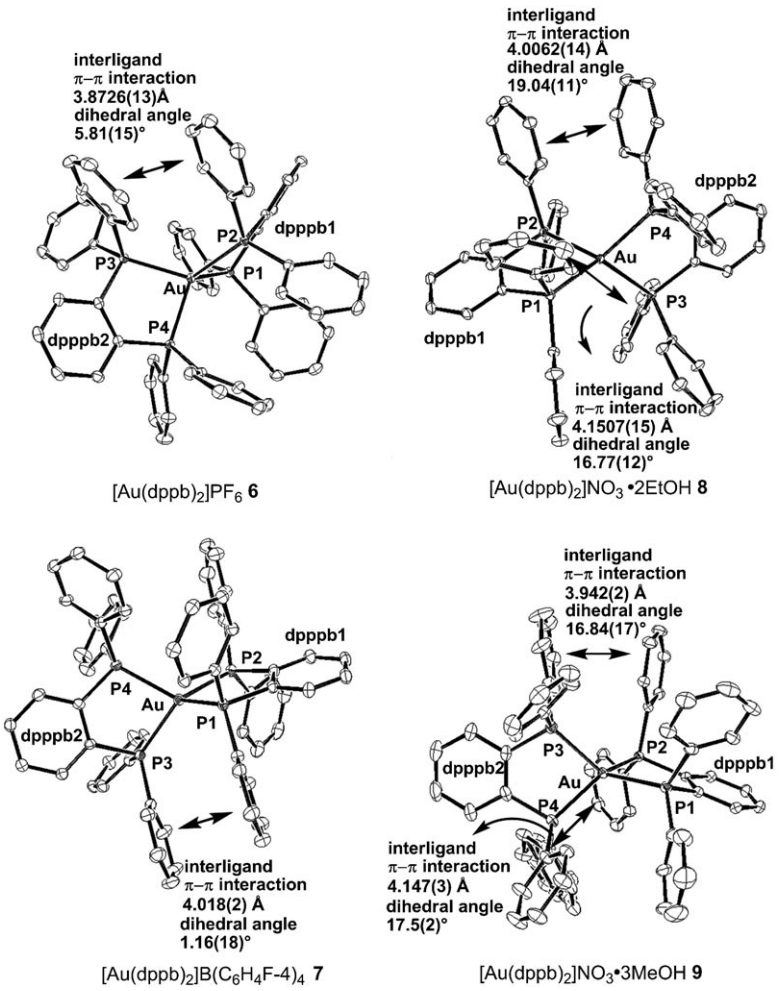

Figure 4. Molecular structures of **6**–**9** in Category II. Thermal ellipsoids are drawn at 50% probability level. Hydrogen atoms and counter anions omitted for clarity.

a space between cationic molecules of gold(I) complexes and, therefore, the stable symmetrical conformation like a structure in Category I can be adopted in the solid state. However, if a counter anion is large, the structure of the cationic molecule can be restricted by the interference of the large anion, and consequently the stable symmetrical structure is suggested to be distorted to an asymmetrical conformation found in Category II. Complex **4**, which has NO_3 as a counter anion, belongs to Category I, but complexes **8** and **9**, the ethanol and methanol adducts of **4**, are in Category II. In single crystals of **8** and **9** the NO_3 anion and methanol or ethanol molecules are incorporated into the crystals and form hydrogen bonds, resulting in the formation of a larger counter anion.

As mentioned above, the size of counter anions seems to be a critical factor determining the conformation of two dppb ligands. The stable symmetrical structures found in Category I would be distorted to an asymmetrical conformation by changing the size of the counter anion, as observed for complexes **4** and **8**.

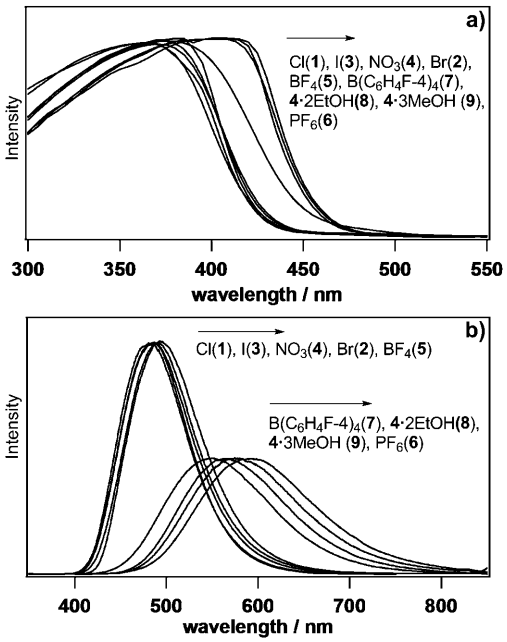

Figure 5. a) Absorption and b) corrected emission spectra of **1–9** in the crystalline state at 293 K. Intensities are adjusted arbitrarily for clarity. $\lambda_{exc} = 350$ nm.

Correlation between structures and photophysical properties of gold(I) complexes: Several studies have been carried out for understanding of the photophysical properties of tetrahedral gold(I) complexes, $[Au(PP)_2]^+$ with diphosphane ligands (PP).[51,61–66] The key units in the tetrahedral $[Au(PP)_2]^+$ responsible for phosphorescence have been regarded as aromatic groups bonded to P atoms, because the lowest energy absorption band must be an emissive state, $\sigma \rightarrow \pi^*$. The valence p orbitals of P ligands are strongly σ antibonding in tetrahedral $[Au(PP)_2]^+$, because the σ orbital is primarily composed of d orbitals (d_{xy}, d_{yz}, d_{xz}) and p orbitals with lone pair electrons.[61]

Figure 5 shows the absorption and emission spectra of **1–9** at 293 K in single crystals. Summarized in Table 1 are the absorption and emission peaks, lifetimes (τ_T), quantum yields (Φ_P), radiative rate constants (k_r), and non-radiative rate constants (k_{nr}), as well as the DFT calculation data with the use of structures obtained by the X-ray analysis. Structural optimizations were not made for these calculations. As listed in Table 1, the emission lifetimes are 0.4–4.0 μs for **1–9**, indicating that these emissions are phosphorescence. The energy difference between HOMO and (HOMO−1) is used as a symmetry index for the two dppb ligands on tetrahedral gold(I) complexes. The index value vanishes under the D_2 symmetry because of the degeneracy of HOMO and (HOMO−1). Thus, the symmetry index is considered to be a measure of distortion of the two dppb ligands from the D_2 symmetry. Owing to the significant distortion from the D_2 symmetry, complexes **6–9** (Category II) exhibit large index values in comparison with those **1–5** in Category I.

The near-colorless complexes **1–5** (Category I) show absorption maxima between $\lambda = 365$ and 380 nm in the solid state (Figure 5a). In contrast, yellow complexes **6–9** (Category II) give the absorption maxima at $\lambda = 385$–420 nm. The red shift of the absorption maxima of Category II compared with that of Category I are consistent with the calculated $S_1 \leftarrow S_0$ energies. Complexes **1–5** (Category I) emit bright blue phosphorescence ($\lambda_{max} = 478$–97 nm). The phosphorescence spectra resemble that of dppb ($\lambda_{max} = 479$ nm) in ap-

Table 1. Photophysical and DFT calculations data of **1–9**.

Complex	λ_{abs}[a] [nm]	S_1 [nm]	λ_{em}[b] [nm]	τ_P [μs]	Φ_P[c]	f_{calcd}[d]	k_r[e]	k_{nr}[f]	HOMO−(HOMO−1) [eV]	HOMO [eV]	LUMO [eV]
Cl (**1**)	365	363	478	3.6	0.86	1.4×10^{-4}	2.4×10^{5}	3.9×10^{4}	0.072	−7.61	−3.45
Br (**2**)	365	359	489	3.2	0.82	1.4×10^{-4}	2.5×10^{5}	5.6×10^{4}	0.054	−7.60	−3.45
I (**3**)	370	353	497	3.3	0.86	0.84×10^{-4}	2.6×10^{5}	5.5×10^{4}	0.029	−7.61	−3.42
NO_3 (**4**)	374	356	486	3.3	0.98	1.1×10^{-4}	3.0×10^{5}	6.1×10^{4}	0.018	−7.64	−3.45
BF_4 (**5**)	380	359	494	4.0	0.90	1.0×10^{-4}	2.3×10^{5}	2.5×10^{4}	0.027	−7.59	−3.44
PF_6 (**6**)	420	393	596	0.36	0.04	1.6×10^{-4}	1.1×10^{5}	2.7×10^{6}	0.64	−7.22	−3.37
$B(C_6H_4F\text{-}4)_4$ (**7**)	385	361	550	2.9	0.55	0.46×10^{-4}	1.9×10^{5}	1.6×10^{5}	0.22	−7.52	−3.41
4·2EtOH (**8**)	410	380	565	0.89	0.32	1.6×10^{-4}	3.7×10^{5}	7.8×10^{5}	0.56	−7.29	−3.40
4·3MeOH (**9**)	407	375	578	0.58	0.23	1.4×10^{-4}	4.0×10^{5}	1.3×10^{6}	0.45	−7.30	−3.35

[a] Absorption maxima. [b] Emission maxima. [c] Absolute photoluminescence quantum yield. [d] Calculated oscillator strength. [e] Radiative rate constant. [f] Non-radiative constant.

pearance, whereas complexes **6–9** (Category II) afford yellow-orange phosphorescence ($\lambda_{max}=550$–596 nm) in single crystals (Figure 5b). The plot of index values [HOMO−(HOMO−1)] versus phosphorescence peak wavelengths is shown in Figure 6. Complexes **1–5** (Category I)

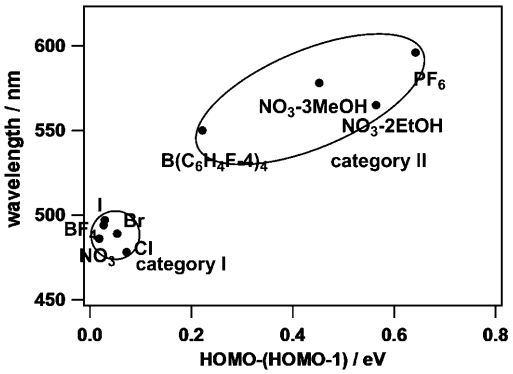

Figure 6. Plot of calculated energy differences [HOMO−(HOMO−1)] and emission maximum wavelengths of **1–9**.

are located on the narrow area at the lower left of the plot. This indicates that the complexes with two symmetrical dppb ligands emit the intense blue phosphorescence. As the index value in Category II increases, the phosphorescence maximum wavelength gets longer. If the two dppb ligands are not equivalent, the degenerated energy level of HOMO will be split, resulting in the destabilization of HOMO energy levels. As shown in Table 1, the LUMO energy levels of **6–9** are in a narrow range between −3.35 and −3.41 eV, whereas the HOMO (σ*) energy levels go up with an increase in the symmetry index. This destabilization of HOMO (σ*) levels is likely responsible for the red shift of the phosphorescence maximum.

With the use of the triplet yield, Φ_{ST}, the phosphorescence yield Φ_P is expressed as Equation (1).

$$\Phi_P = \Phi_{ST}\, k_r\, \tau_T \quad (1)$$

From Equation (1), the k_r at T_1 state is formulated by Equation (2).

$$k_r = \Phi_P/(\tau_T\, \Phi_{ST}) \quad (2)$$

On the assumption that $\Phi_{ST}=1.0$, the k_r values for **1–9** are obtained as 1.1–$4.0\times10^5\ s^{-1}$ at 293 K, indicating that the k_r values of the complexes in Category I are similar to those in Category II. This result agrees with trend in the oscillator strengths of **1–9** at 300 K obtained from DFT calculations (Table 1).

As listed in Table 1, the phosphorescence yields of **6–9** (Category II) are considerably smaller than those of the complexes in Category I. Furthermore, the complexes in Category II have nonradiative rate constants, k_{nr}, larger than those in Category I. Presumably, the conformational differences in the dppb ligand of the complexes between two categories afford a large effect on their k_{nr} values. The asymmetrical CH/F, CH/O, OH/O, and CH/π interactions between $[Au(dppb)_2]^+$ and counter anions, which make two dppb ligands nonequivalent in crystals of **6–9**, are likely responsible for the radiationless processes peculiar to the phosphorescent triplet state of the complexes in Category II.

According to DFT calculations, the emitting states of complexes **1–9** are mainly CT states from P atom to phenylene and phenyl groups of dppb ligands. Though the MLCT character responsible for Jahn–Teller effect is not so strong, 12–14% for **1–9**, these complexes are not emissive in degassed solutions at room temperature.

The symmetrical coordination of two dppb ligands to the Au^I atom is necessary for the intense blue phosphorescence on tetrahedral gold(I) complexes. We consider that the intra-ligand π–π interactions in the complexes of Category I attribute to the symmetrical coordination geometry of the cationic molecule. A small conformational change of two dppb ligands of the complexes in Category II is caused by the large counter anion, leading to the symmetry reduction and thus, the resulting destabilization of HOMO (σ*) levels dramatically alter the optical properties of the gold(I) complexes in the crystalline state.

Photophysical properties of tetrahedral gold(I) complexes in EtOH at 77 K: Figure 7 shows the phosphorescence spectra of **1**, **4**, and **6** in EtOH glasses at 77 K, obtained with excitation at $\lambda=350$ nm. Complexes **1**, **4**, and **6** exhibit very similar phosphorescence spectra with emission maxima at $\lambda=504$ nm, regardless of the sizes of counter anions. Presumably, the cationic phosphorescent moiety is free from the effects of the counter anions in dilute frozen solutions at 77 K. Another notable feature is that emission spectra are broad and extend up to $\lambda=600$ nm. This observation suggests that, at least, two emitting species exist in the frozen solutions. In fact, as shown in Figure 7, the phosphorescence spectrum of **1** in ethanol at 77 K is well interpreted as a sum of the two

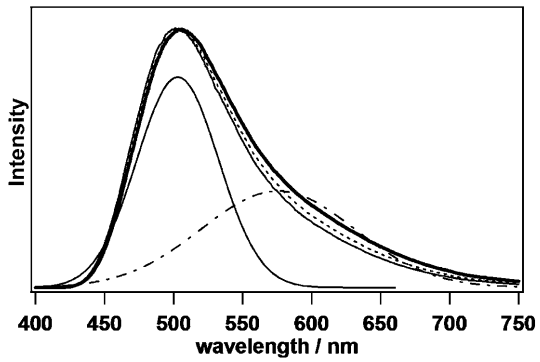

Figure 7. Corrected emission spectra of **1** (bold), **4** (dotted), and **6** (solid) in EtOH glasses at 77 K. $\lambda_{exc}=350$ nm. Two segmentalized spectra (solid and dashed) from **1**.

spectra: one has a peak at $\lambda = 502$ nm (solid), and the other, at $\lambda = 575$ nm (dashed).

The following observation further confirms the presence of the two emitting species in the ethanol glasses at 77 K.

Analysis of Figure 8 reveals 1) the phosphorescence spectra of **1** in EtOH glasses at 77 K, measured by changing the excitation wavelength from $\lambda = 340$ to 395 nm and 2) the excitation spectra monitored at $\lambda = 500$ and 600 nm. Similar measurements were carried out for **4** and **6**, as shown in Figures S6 and S7. As the exciting wavelength is increased, a new orange emission is observed around $\lambda = 600$ nm. The excitation spectrum monitored at $\lambda = 500$ nm (dashed) is slightly blue shifted in comparison with that at $\lambda = 600$ nm (bold). These results again suggest that two emitting species exist in the solution. We found that the phosphorescence spectra were independent of the concentrations (5×10^{-6}–10^{-4} M) of the complexes. Thus, aggregation is not responsible for the formation of the two emitting species. Probably, the cationic phosphorescent moiety free from the anion has two conformers in the solution at 77 K. The observations made for the ethanol glasses at 77 K are summarized as 1) two phosphorescent conformers, which give blue and orange emissions, exist in the solution, and 2) although the excitation spectra of the two conformers are very similar each other, the gap in the phosphorescence peak wavelengths is as large as ≈ 100 nm. It is likely that both S_0 and S_1 energies are close between the two conformers and, however, the T_1 energy markedly differs between them.

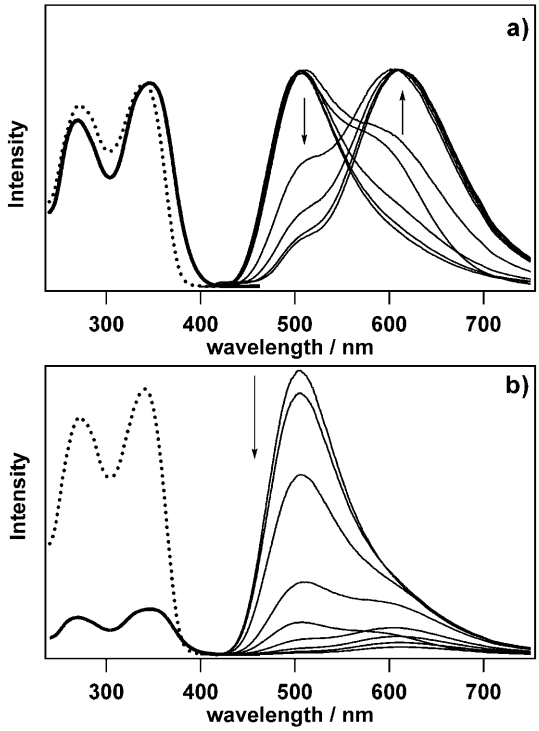

Figure 8. Exciting-wavelength dependence of **1** in EtOH glasses at 77 K, one measurement every 10 nm from $\lambda = 340$ to 370 nm and every 5 nm from $\lambda = 370$ to 395 nm; a) after being normalized and b) before being normalized. Excitation spectra; $\lambda = 500$ nm (bold) and $\lambda = 600$ nm (dashed).

Unlike the crystalline state, there is equilibrium between two conformers in dilute frozen EtOH glasses at 77 K: a blue-emitting conformer classified into Category I and a yellow orange emitting conformer, into Category II.

Reversible vapoluminescent response of complex 4: Complex **4** (Category I) shows the intense blue phosphorescence at $\lambda_{max} = 486$ nm. However, the ethanol (**8**) and methanol (**9**) adducts of **4** display yellow-orange phosphorescence with peak wavelengths at $\lambda_{max} = 565$ and 578 nm, respectively (Figure 9). During the course of this study, we found that yellow single crystals of **8** or **9** undergo solvent loss in an oven by heating at 100 °C for 20 min. The yellow single crystals then change to white, fragile solids, which are unsuitable for single-crystal X-ray analysis, resulting in the phosphorescence color change from yellow orange to blue. If the fragile solids are exposed to alcohol vapors, the color turns from white to yellow concomitantly with the phosphorescence color change from blue to yellow orange. These results indicate that the reversible vapochromic reaction takes place for the complexes, **8** and **9**. The identification of the fragile solids obtained from **8** has been carried out by X-ray powder diffraction (XRD) measurements, and the cell constants were refined by the Pawley method (see Table S18 in

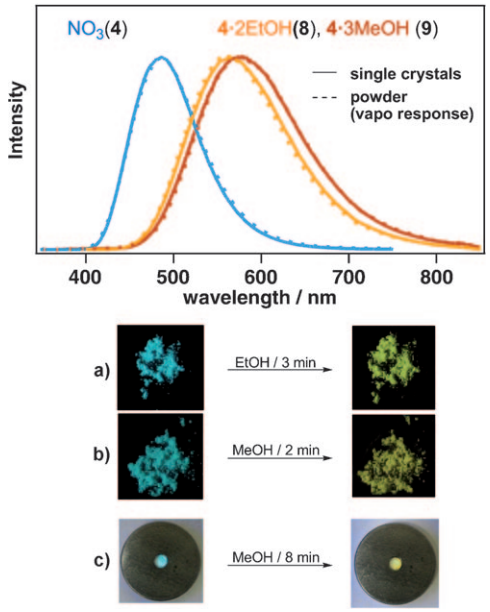

Figure 9. Corrected emission spectra of **4** (blue), **8** (orange) and **9** (red); single crystals (solid), powder (dotted) ($\lambda_{exc} = 350$ nm). Emission color changes images upon UV irradiation ($\lambda_{exc} = 365$ nm); a) **4** in the powder state upon the diffusion of EtOH, b) **4** in powder state upon the diffusion of MeOH, and c) 0.5% mixture of **4** in a matrix of KBr upon the diffusion of MeOH.

the Supporting Information). Analysis of Figure 10a reveals that the powder diffraction patterns of the fragile solids from **8**, are well fitted as the single phase with similar cell constants to those of **4**, leading to the conclusion that the loss of ethanol molecules from the single crystals **8** by heating at 100 °C results in the formation the complex **4**.

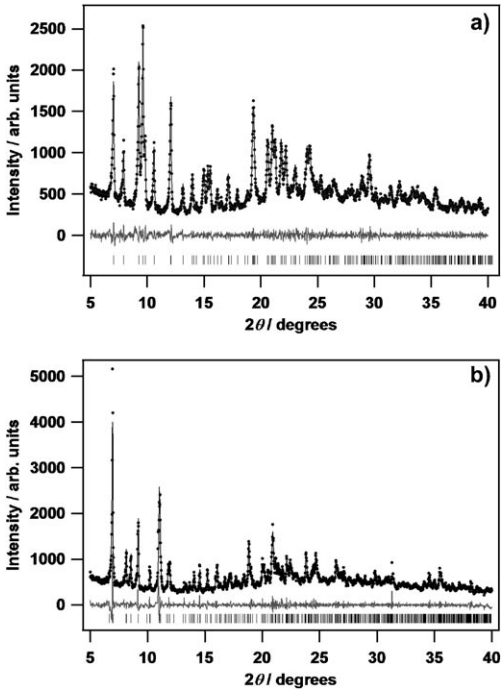

Figure 10. XRD patterns; a) the white fragile solids from **8** b) after exposure to ethanol vapor. Observed (dotted) and calculated (solid) profiles, difference plot (gray) [$(I_{obs}-I_{calcd})$] of the Pawley refinement, and peak positions (solid bar) (2θ range 5.0–40°).

As mentioned above, the white fragile solids obtained by heating of **8** turn yellow by exposure to the ethanol vapor, and the phosphorescence color changes from blue to yellow orange. The phosphorescence spectrum with a peak at $\lambda_{max}=$ 564 nm is in good agreement with that of **8** in the crystalline state (Figure 9). The yellow powder is identified as **8** by using XRD (Figure 10b and Table S18 in the Supporting Information). The phosphorescence color alteration from blue to yellow orange occurs within 3 min of exposure to ethanol vapor. Conversely, the yellow-orange phosphorescence returns to blue by heating in an oven at 100 °C after ≈20 min. This vapochromic response is fully reproducible without chemical degradation of the complexes (Scheme 2).

The vapochromic response was examined with the use of a variety of solvent vapors. We found that only methanol and ethanol vapors reproduce the phosphorescence color changes. The response times for methanol and ethanol were, respectively, less than 2 min and ≈3 min (Figure 9a,b). It is assumed that the small sized VOC, methanol, is more suitable than ethanol to approach the NO_3 anion surrounded by $[Au(dppb)_2]$ cations in crystal. White fragile solid were exposed to a series of vapors having an OH group, 1-propamol, 2-propanol, 1-butanol and water at room temperature. No vapoluminescence was observed for these vapors. This result is explained by assuming that these solvent molecules are unable to soak into the fragile solids: the former three are too large in size and the latter is too hydrophilic to interact with the fragile solids.

No vapochromic response was observed for the complex **4** in the single crystalline state. However, the powdered complex **4**, obtained by grinding the crystals in an agate mortar with a pestle, can exhibit vapochromism. Presumably, methanol and ethanol molecules are unable to disperse inside the single crystals. Defects, such as cracks located on the surface of crystals, are necessary for invasion of the alcohol molecules.

Complex **4** can be used as a dopant for vapoluminescent response.[13] A doped sample was prepared as a disk for IR spectroscopy; a 0.5% mixture (w/w) of **4** in a matrix of finely ground KBr. This sample shows same vapochromic response as neat powder samples of **4** (Figure 9c).

Mechanoluminescent response of complex 1–9: Upon grinding microcrystalline powders of **5** in an agate mortar with a pestle, the color of the ground portion in the mortar is changed from white to yellow (Figure 11B) and the intense blue phosphorescence of **5** (Figure 11A) changes to weak yellow-orange color (Figure 11C). After continuous grinding of the whole sample for an hour, the phosphorescence color eventually changed from blue ($\lambda_{max}=$494 nm, Figure 11A) to

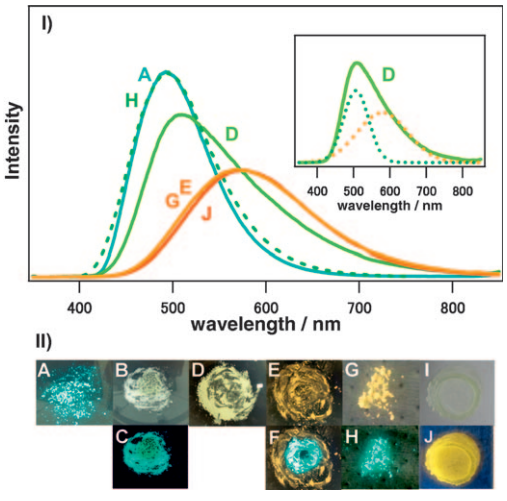

Figure 11. **I**) Corrected emission spectra ($\lambda_{exc}=$350 nm) and **II**) images upon UV irradiation (except for B and I) in various states of **5** (A–J, see text). The inset shows two segmentalized spectra in state D.

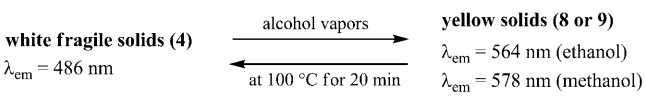

Scheme 2. Reversible vapochromic responses.

yellow orange ($\lambda_{max}=575$ nm, Figure 11E) through a yellow-emitting state (Figure 11D). A reversible transformation from a yellow-orange-emitting form to a blue-emitting form is observed by treating the sample with diethyl ether (Figure 11F). Furthermore, this yellow-orange-emitting form (Figure 11E) was found to show vapochromism. Upon exposure of this form (Figure 11G) to the vapors of VOCs (ether, acetone, acetonitrile, dichloromethane, and tetrahydrofuran) under ambient temperature, the phosphorescence turns from yellow orange to intense blue within 0.5–5 min (Figure 11H). The blue phosphorescence spectrum is very close to that of **5** with a peak at $\lambda_{max}=494$ nm.

The emission spectrum of a yellow-emitting state (Figure 11D) is very similar in shape to those in EtOH glasses at 77 K (Figure 7). The spectrum is interpreted in terms of a sum of the two spectra: one has a peak maxima at $\lambda=$ 505 nm (blue green) and another, $\lambda=575$ nm (orange) (inset in Figure 11), indicating that this intermediate state consists of the starting complex **5** and a yellow-orange-emitting form. This form can be classified into Category II, because of the long wave emission ($\lambda=575$ nm), the low quantum yield (0.13), and the short lifetime (0.62 μs). Thus we can conclude that the stable symmetrical structure of **5** in Category I is distorted to an asymmetrical conformation in Category II by grinding. The excitation spectrum monitored at $\lambda=575$ nm in the state of Figure 11E is similar to that of **9** at $\lambda=578$ nm and has an asymmetrical configuration. This supports the suggestion of conformation change of the solid **5** with grinding (see Figure S8 in the Supporting Information).

A yellow-orange-emitting form of **5** is displayed without grinding if the dichloromethane solution of **5** is deposited on a quartz plate. After slow evaporation of dichloromethane, the pale-yellow-quartz plate was kept in a dried box at 293 K for 12 h (Figure 11I). The phosphorescence spectrum of the deposited sample is very similar to that of the ground sample of **5** (Figure 11E, G, and J). This deposited sample shows the same response to ether as seen in ground **5** solid.

The XRD patterns at various states have been shown in Figure 12. The cell constants from the powder diffraction pattern of the complex after lightly ground for the XRD measurement is consistent with those from those of single crystal analysis of **5** (Figure 12A and Table S18). On going to fine powders, the peak intensities in the XRD pattern gradually decrease and become broad (Figure 12D). Eventually, the amorphous phase in its entirety is revealed (Figure 12E). State D is clearly composed of both the crystalline phase (Figure 12A) and the amorphous phase (Figure 12E) based on the analysis of XRD patterns. The fact that the emission spectrum in state D, is interpreted in terms of a sum of two spectra (in state A and state E) is consistent with this result. The distortion of molecules, which result in an asymmetrical conformation, probably occurs by mechanical stimulus. In the amorphous phase, there are almost no regular intermolecular interactions to govern the packing structure in the crystalline state. Analysis of the deposited sample (Figure 11I) also reveals amorphous phase, as a throughout the XRD patterns (Figure S9).

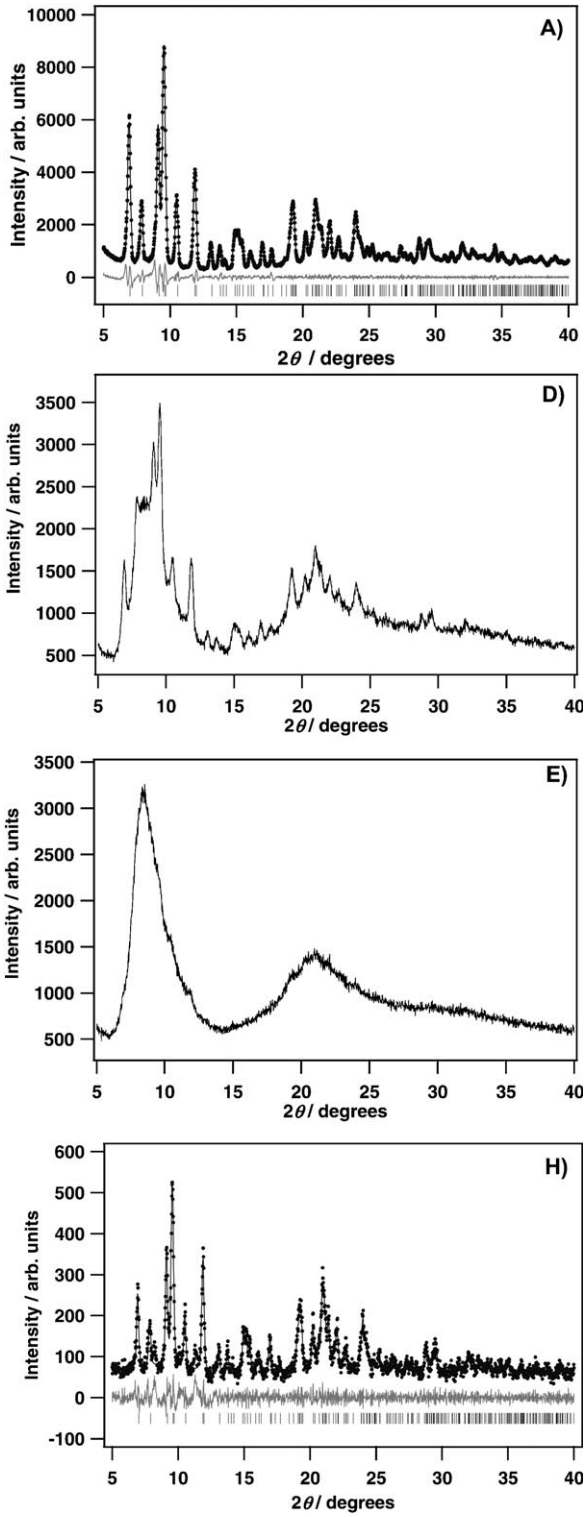

Figure 12. XRD patterns of **5** in A, D, E, and H states (see text and Figure 11). Observed (dotted for A and H, solid for D and E) and calculated (solid for A and H) profiles, difference plot (gray for A and H) [$(I_{obs}-I_{calcd})$] of the Pawley refinement, and peak positions (solid bar for A and H) (2θ range 5.0–40°).

In recent reports,[43–46] the transformation from the crystal phase to amorphous phase is a key process for appearance

of mechanoluminescent response. The sample after treatment with the ether vapor exhibits an XRD pattern identical with that of **5** (Figure 12H and Table S18).[67] In this response the VOCs are the stimuli for the conversion from the amorphous state to a more stable crystalline state. Accordingly, this vapochromic response is irreversible. However, it is confirmed that the color alteration cycles consisting of blue to yellow-orange phosphorescence (mechanochromism) and yellow-orange to blue phosphorescence (vapochromism) are repeatable.

We have studied the mechanoluminescent response of the complex **4**. Continuous grinding of **4** in the crystalline state (Figure 13A) for a prolonged period does not produce an amorphous state throughout its entirety and, ultimately, affords "a mechanical equilibrium" (Figure 13B): the blue emitting complex, **4**, still emerges by locally strong rubbing even after long grinding (Figure S10). These observations suggest that reversible transformation, amorphous↔crystalline, occurs by grinding of the complex **4**.

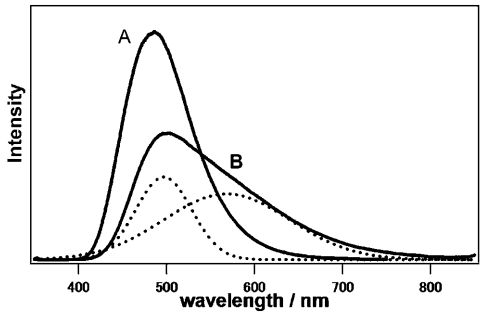

Figure 13. Corrected emission spectra of **4** ($\lambda_{exc}=350$ nm); A) before grinding, B) after grinding.

On the other hand, the ethanol (**8**) and methanol (**9**) adducts of **4** have shown smooth transformation from the crystal phase to the amorphous state within 10 min grinding (Figure S11 and S12). This result would support for the symmetry reduction of two dppb ligands during the transformation from the crystalline state to the amorphous state by grinding because **8** and **9** originally have two asymmetric ligands.

Other complexes **1**–**3** (Category I) and **6** and **7** (Category II) show similar mechanoluminescent responses by grinding (Figure S13–S17). In the amorphous state, the complexes have almost identical photophysical properties independent of counter anions: the phosphorescence peaks are located at $\lambda=571$–578 nm and the quantum yields are in the range 0.11–0.14. It is noteworthy that most complexes exhibit the red shift of phosphorescence maxima and the lowering of quantum yields by grinding. An exceptional case is complex **6**: the phosphorescence peak located at $\lambda=596$ nm in the crystalline state is blue shifted to $\lambda=575$ nm in the amorphous state. Further, the quantum yield in the amorphous state is increased by three times, as compared with that in the crystalline state.

Conclusion

We have reported phosphorescence color alteration of tetrahedral gold(I) complexes, $[Au(dppb)_2]^+$ in the crystalline state by exchanging counter anions. The symmetrical coordination of two dppb ligands to Au^I atom is confirmed to be necessary for the intense blue phosphorescence on the basis of the correlation between the structure of the cationic molecule and the emission color. The counter anion governs the photophysical property of the cationic complex through intermolecular interactions in crystalline state. In fact, all complexes show the same property in dilute EtOH glasses at 77 K irrespective of the nature of the counter anions. From the DFT calculations, a symmetry reduction of two dppb ligands, which is caused by changing counter anions, is found to result in the destabilization of HOMO (σ^*) levels, leading to a red shift of the phosphorescence maximum. We have also demonstrated that the symmetry reductions are responsible for the phosphorescence color alteration caused by external stimuli (VOCs, mechanical grinding). The unique photophysical character of $[Au(dppb)_2]^+$ is principally ascribed to the nature of dppb ligand.

Experimental Section

Materials: The ligand dppb was obtained from Wako Chemicals. Chemicals $[Au(SMe_2)]Cl$, KBr, KI, KNO_3, NH_4PF_4, KPF_6, and $NaB(C_6H_4F\text{-}4)_4$ [sodium tetrakis(4-fluorophenyl)borate] were obtained from Aldrich. The complex $[Au(PPh_3)]Cl$ was prepared according to the literature procedure.[68]

Synthesis of $[Au(dppb)_2]Cl$ (1): To a THF solution (3 mL) of $[Au(PPh_3)]Cl$ (0.15 g, 0.03 mmol) was slowly added dppb (0.268, 0.06 mmol). After 20 min of standing, colorless plate single crystals were obtained (0.29 g, 89%). ^1H NMR (400 MHz, CD_2Cl_2, 293 K): $\delta=7.542$–7.451 (m, 8H, *o*-phenylene), 7.342–7.306 (m, 8H, phenyl), 7.108–7.025 ppm (m, 32H, phenyl); $^{31}P\{^1H\}$ NMR (160 MHz, CD_2Cl_2, 293 K): $\delta=21.80$ ppm (s); elemental analysis calcd (%) for $C_{60}H_{48}AuClP_4$ (1125.34): C 64.04, H 4.30; found: C 63.86, H 4.39.

Synthesis of $[Au(dppb)_2]Br$ (2): To a CH_2Cl_2 solution (10 mL) of $[Au(dppb)_2]Cl$ (**1**) (0.20 g, 0.18 mmol) was added an aqueous KBr solution (1N, 10 mL). After 2.0 h, the CH_2Cl_2 layer was evaporated to dryness. Recrystallization of the crude product from the THF solution afforded analytical pure colorless crystals (0.17 g, 82%). ^1H NMR (400 MHz, CD_2Cl_2, 293 K): $\delta=7.355$–7.289 (m, 8H, *o*-phenylene), 7.122–7.030 (m, 8H, phenyl), 7.111–7.029 ppm (m, 32H, phenyl); $^{31}P\{^1H\}$ NMR (160 MHz, CD_2Cl_2, 293 K): $\delta=21.83$ ppm (s); elemental analysis calcd (%) for $C_{60}H_{48}AuBrP_4$ (1169.79): C 61.60, H 4.14; found: C 61.77, H 4.22.

Synthesis of $[Au(dppb)_2]I$ (3): This compound was prepared similarly to $[Au(dppb)_2]Br$ (**2**), except that an aqueous KI solution (1N, 10 mL) was used instead of KBr. Analytically pure material was obtained by addition of Et_2O on the surface of the CH_2Cl_2 solution. Yield: 0.15 g of colorless crystals (69%). ^1H NMR (400 MHz, CD_2Cl_2, 293 K): $\delta=7.385$–7.289 (m, 8H, *o*-phenylene), 7.122–7.025 (m, 8H, phenyl), 7.116–7.029 ppm (m, 32H, phenyl); $^{31}P\{^1H\}$ NMR (160 MHz, CD_2Cl_2, 293 K): $\delta=21.83$(s); elemental analysis calcd (%) for $C_{60}H_{48}AuIP_4$ (1216.81): C 59.22, H 3.98; found: C 59.39, H 3.87.

Synthesis of $[Au(dppb)_2]NO_3$ (4): This compound was prepared similarly to $[Au(dppb)_2]Br$ (**2**), except that an aqueous KNO_3 solution (1N, 10 mL) was used instead of KBr. Analytically pure material was obtained by addition of Et_2O on the surface of the CH_2Cl_2 solution. Yield: 0.16 g of colorless solid (80%). ^1H NMR (400 MHz, CD_2Cl_2, 293 K): $\delta=7.510$–7.238

(m, 8H, *o*-phenylene), 7.312–7.346 (m, 8H, phenyl), 7.115–7.028 ppm (m, 32H, phenyl); $^{31}P\{^1H\}$ NMR (160 MHz, CD_2Cl_2, 293 K): $\delta = 21.81$ ppm (s); elemental analysis calcd (%) for $C_{60}H_{48}AuNO_3P_4$ (1151.89): C 62.56, H 4.20; found: C 62.29, H 4.07.

Synthesis of [Au(dppb)$_2$]BF$_4$ (5): This compound was prepared similarly to [Au(dppb)$_2$]Br (**2**), except that an aqueous NH_4BF_4 solution (1N, 10 mL) was used instead of KBr. Analytically pure material was obtained by recrystallization from ethanol. Yield: 0.16 g of colorless solid (77%). ^1H NMR (400 MHz, CD_2Cl_2, 293 K): $\delta = 7.542$--7.451 (m, 8H, *o*-phenylene), 7.342–7.306 (m, 8H, phenyl), 7.108–7.025 ppm (m, 32H, phenyl); $^{31}P\{^1H\}$ NMR (160 MHz, CD_2Cl_2, 293 K): $\delta = 21.80$ ppm (s); elemental analysis calcd (%) for $C_{60}H_{48}AuBF_4P_4$ (1176.69): C 61.24, H 4.11; found: C 61.34, H 3.96.

Synthesis of [Au(dppb)$_2$]PF$_6$ (6): This compound was prepared similarly to [Au(dppb)$_2$]Br (**2**), except that the aqueous KPF_6 solution (1N, 10 mL) was used instead of KBr. Analytically pure material was obtained by recrystallization from methanol. Yield: 0.18 g of pale yellow solid (82%). ^1H NMR (400 MHz, CD_2Cl_2, 293 K): $\delta = 7.537$–7.4337 (m, 8H, *o*-phenylene), 7.337–7.301 (m, 8H, phenyl), 7.106–7.025 ppm (m, 32H, phenyl); $^{31}P\{^1H\}$ NMR (160 MHz, CD_2Cl_2, 293 K): $\delta = 21.85$ ppm (s); elemental analysis calcd (%) for $C_{60}H_{48}AuF_6P_5$ (1234.85): C 58.36, H 3.92; found: C 58.52, H 3.79.

Synthesis of [Au(dppb)$_2$]B(C$_6$H$_4$F-4)$_4$ (7): This compound was prepared similarly to [Au(dppb)$_2$]Br (**2**), except that an aqueous $NaB(C_6H_4F\text{-}4)_4$ solution (1N, 10 mL) [$NaB(C_6H_4F\text{-}4)_4$ = sodium tetrakis(4-fluorophenyl) borate] was used instead of KBr. Analytically pure material was obtained by recrystallization from ethanol. Yield: 0.18 g of pale yellow solid (82%). ^1H NMR (400 MHz, CD_2Cl_2, 293 K): $\delta = 7.223$–7.396 (m, 8H, *o*-phenylene), 7.250–7.313 (m, 8H, phenyl), 7.083–7.007 ppm (m, 32H, phenyl); $^{31}P\{^1H\}$ NMR (160 MHz, CD_2Cl_2, 293 K): $\delta = 21.81$ ppm (s); elemental analysis calcd (%) for $C_{84}H_{64}AuBF_4P_4$ (1481.07): C 68.12, H 4.36; found: C 68.52, H 3.79.

Synthesis of [Au(dppb)$_2$]NO$_3$·2EtOH (8): This compound was obtained by recrystallization of **4** (200 mg, 0.17 mmol) from ethanol at ambient temperature. Yield: 0.14 g of colorless solid (65%). ^1H NMR (400 MHz, CD_2Cl_2, 293 K): $\delta = 7.510$–7.238 (m, 8H, *o*-phenylene), 7.312–7.346 (m, 8H, phenyl), 7.115–7.028 (m, 32H, phenyl), 3.725 (q, 4H, $J = 7.01$ Hz, CH_3CH_2OH), 1.245 ppm (t, 6H, $J = 6.96$ Hz, CH_3CH_2OH); $^{31}P\{^1H\}$ NMR (160 MHz, CD_2Cl_2, 293 K): $\delta = 21.81$ ppm(s); elemental analysis calcd (%) for $C_{64}H_{60}AuNO_5P_4$(1244.03): C 61.79, H 4.86; found: C 61.33, H 4.73.

Synthesis of [Au(dppb)$_2$]NO$_3$·3MeOH (9): This compound was obtained by recrystallization of **4** (200 mg, 0.17 mmol) from methanol at 0°C. Yield: 0.16 g of colorless solid (48%). ^1H NMR (400 MHz, CD_2Cl_2, 293 K): $\delta = 7.583$–7.453 (m, 8H, *o*-phenylene), 7.355–7.324 (m, 8H, phenyl), 7.123–7.050 (m, 32H, phenyl), 3.424 (d, 3H, $J = 5.38$, CH_3OH), 1.274 ppm (q, 1H, $J = 5.63$, CH_3OH); $^{31}P\{^1H\}$ NMR (160 MHz, CD_2Cl_2, 293 K): $\delta = 21.81$ ppm (s); elemental analysis calcd (%) for $C_{63}H_{60}AuNO_6P_4$(1248.02): C 61.21, H 4.85; found: C 60.89, H 4.62.

Crystal structure determination: The crystallographic data and the results of the structure refinements are summarized in Tables S1 and S2. In the reduction of data, Lorentz and polarization corrections and empirical absorption corrections were made.[69] The structures were solved by the direct method (SIR2004).[70] All non-hydrogen atoms were refined with anisotropic thermal parameters. Hydrogen atoms were fixed at calculated positions. CCDC-702673 (**1**), CCDC-777271 (**2**), CCDC-777272 (**3**), CCDC-777273 (**4**), CCDC-733922 (**5**), CCDC-702674 (**6**), CCDC-777274 (**7**), CCDC-777275 (**8**), and CCDC-777276 (**9**) contain the supplementary crystallographic data for this paper. These data can be obtained free of charge from the Cambridge Crystallographic Data Centre via www.ccdc.cam.ac.uk/data_request/cif.

X-ray powder diffraction: Single crystals or dried powder samples were lightly ground in an agate mortar and pestle and mounted on a glass sample holder, powder diffraction patterns were measured by using a RIGAKU SmartLab diffractometer with $Cu_{K\alpha}$ radiation. Powder diffraction patterns were collected between 2θ of 5 and 40° with a 2θ stepping angle of 0.02°.

Vapoluminescent studies: The sample on a quartz slide was exposed to a saturated atmosphere of solvent vapor in a petri dish.

General: ^1H NMR, and ^{31}P NMR spectroscopy samples were recorded in CD_2Cl_2 by using a JEOL EX-400 and a JEOL EX-500. Single crystals or powder samples of dppb, **1**–**9** in quartz petri dishes or quartz tubes (5ϕ) were used for all optical measurements in the solid state. Solid state absorption spectra were recorded by using an upgraded JASCO MSV-350. The excitation and emission spectra were recorded at room temperature and at 77 K by using a Hitachi F-7000. The light-intensity distribution of a Xenon lamp has been corrected with the use of Rodamine B in ethyleneglycole and the output of photomultiplier has been calibrated in the wavelength range 300–850 nm, by using a secondary standard lamp. Laser photolysis studies were carried out with the use of a Nd:YAG laser (Sure Light 400 from Hoya Continuum Ltd.) equipped with second, third, and forth harmonic generators. A third harmonic excitation light for the lifetime measurements was used ($\lambda = 355$ nm): the duration and the energy of the laser pulse are 5 ns and 30 mJ pulse^{-1}, respectively. The monitoring system for the decay of emission has already been reported elsewhere.[71] Solid-state emission quantum yields at room temperature and at 77 K were determined with an absolute PL quantum yield measurement system, C-9920–02G (HAMAMATSU).

Computational details: Calculations were performed by using density-functional theory (DFT)[72] with Gaussian03.[73] Beck three-parameter Lee–Yang–Parr exchange-correlation functional of B3LYP[74,75] was employed. The LANL2DZ effective core potentials and valence basis set[76] were used along with two f-type polarization functions with the exponents $a_f = 0.2$ and $a_f = 1.19$[77] and the Couty–Hall *p*-type functions[78] to describe the valence electrons of gold. Main group elements were described with the LANL2DZ basis set and additional polarization functions were added to P ($a_d = 0.34$). The combination of functional and basis sets was chosen on the basis of a series of test calculations on the ground state singlet of $[Au(PH_3)_3]^+$[79] The calculations of excitation energies and oscillator strengths were carried out with TD DFT at the B3LYP/LANL2DZ level.

A compact orbital representation for the electronic transition density matrix[80] is calculated to interpret the qualitative nature of the lowest triplet (T_1) state. The transition density matrix is given by $T_{ia} = \langle\phi_i|\hat{T}|\phi_a\rangle$, for which ϕi and ϕa are occupied and virtual molecular orbitals, respectively. The natural transition orbitals (NTOs) are obtained by the orbital transformation followed by a singular value decomposition of the ($n_{occ} \times n_{virt}$) transition density matrix. In the NTO representation, the electronic transitions can be expressed by one single "electron-hole" pair with an associated eigenvalue of essentially one, even such transitions that are highly mixed in the canonical molecular orbital basis. This procedure gives us a simple orbital interpretations of "what got excited to where". The "hole" and "electron" approximately correspond to HOMO and LUMO, respectively in the dppb ligand.

The magnitudes of spin-orbit interaction among the excited states are lower than 1000 cm^{-1} in most cases and much smaller than the electronic excitation energies calculated by TD DFT. Thus a perturbation technique is a appropriate one for the evaluation of the phosphorescence states. A perturbed wave function Ψ, which describes a phosphorescence state is thus represented as a linear combination of the unperturbed wave functions ψk, viz., $\Psi = \sum c_k\psi_k$. According to the perturbation theory for degenerate states, the perturbation energy E_{so} and the coefficients vector C are calculated by solving the eigenvalue problem as $(\langle\psi|H_{so}|\psi\rangle - E_{so}I)C = 0$, in which H_{so} is the spin-orbit operator and I is the unit matrix. In the evaluation of the spin-orbit molecular integrals, we employed the atomic orbital coefficients for natural atomic orbitals,[81] which are obtained by NBO3.0[82] included in Gaussian03. All the quantum chemical calculations were carried out on a Fujitsu PC cluster system. The calculations of NTO and excited states with spin-orbit coupling were performed using a lab-made code.

Acknowledgements

This research was partly supported by "Incentive Research Grant" (RIKEN).

[1] Y. Sagara, T. Kato, *Nat. Chem.* **2009**, *1*, 605–610.
[2] G. Zhang, G. M. Palmaer, M. W. Dewhirst, C. L. Fraser, *Nat. Mater.* **2009**, *8*, 747–751.
[3] M. A. Mansour, W. B. Connick, R. J. Lachicotte, H. J. Gysling, R. Eisenberg, *J. Am. Chem. Soc.* **1998**, *120*, 1329–1330.
[4] S. M. Drew, D. E. Janzen, C. E. Buss, D. I. MacEwan, K. M. Dublin, K. R. Mann, *J. Am. Chem. Soc.* **2001**, *123*, 8414–8415.
[5] C. E. Buss, K. R. Mann, *J. Am. Chem. Soc.* **2002**, *124*, 1031–1039.
[6] R. L. White-Morris, M. M. Olmstead, F. Jiang, D. S. Tinti, A. L. Balch, *J. Am. Chem. Soc.* **2002**, *124*, 2327–2336.
[7] M. Kato, A. Omura, A. Toshikawa, S. Kishi, Y. Sugimoto, *Angew. Chem.* **2002**, *114*, 3315–3317; *Angew. Chem. Int. Ed.* **2002**, *41*, 3183–3185.
[8] V. W.-W. Yam, K. M.-C. Wong, N. Zhu, *J. Am. Chem. Soc.* **2002**, *124*, 6506–6507.
[9] R. L. White-Morris, M. M. Olmstead, A. L. Balch, *J. Am. Chem. Soc.* **2003**, *125*, 1033–1040.
[10] H. V. R. Dias, H. V. K. Diyabalanage, M. A. Rawashdeh-Omary, M. A. Franzman, M. A. Omary, *J. Am. Chem. Soc.* **2003**, *125*, 12072–12073.
[11] W. Lu, M. C. W. Chan, N. Zhu, C.-M. Che, Z. He, K.-Y. Wong, *Chem. Eur. J.* **2003**, *9*, 6155–6166.
[12] L. J. Grove, J. M. Rennekamp, H. Jude, W. B. Connick, *J. Am. Chem. Soc.* **2004**, *126*, 1594–1595.
[13] T. J. Wadas, Q.-M. Wang, Y.-J. Kim, C. Flaschenreim, T. N. Blanton, R. Eisenberg, *J. Am. Chem. Soc.* **2004**, *126*, 16841–16849.
[14] M. Kato, *Bull. Chem. Soc. Jpn.* **2007**, *80*, 287–294.
[15] P. Du, J. Schneider, W. W. Brennessel, R. Eisenberg, *Inorg. Chem.* **2008**, *47*, 69–77.
[16] L. J. Grove, A. G. Oliver, J. A. Krause, W. B. Connick, *Inorg. Chem.* **2008**, *47*, 1408–1410.
[17] J. Forniés, S. Fuertes, J. A. Loópez, A. Martiín, V. Sicilia, *Inorg. Chem.* **2008**, *47*, 7166–7176.
[18] M. L. Muro, C. A. Daws, F. N. Castellano, *Chem. Commun.* **2008**, 6134–6136.
[19] J. Ni, L. Y. Zhang, H. M. Wen, Z. N. Chen, *Chem. Commun.* **2009**, 3801–3803.
[20] J. Ni, Y. H. Wu, X. Zhang, B. Li, L. Y. Zhang, Z. N. Chen, *Inorg. Chem.* **2009**, *48*, 10202–10210.
[21] J. S. Field, G. D. Grimmer, O. Q. Munro, B. P. Waldron, *Dalton Trans.* **2010**, *39*, 1558–1567.
[22] P. Du, *Inorg. Chim. Acta* **2010**, *363*, 1355–1358.
[23] E. J. Fernández, J. M. Lopez-de-Luzuriaga, M. Monge, M. E. Olmos, J. Perez, A. Laguna, A. A. Mohamed, J. P. Fackler, Jr., *J. Am. Chem. Soc.* **2003**, *125*, 2022–2023.
[24] J. Lefebvre, R. J. Batchelor, D. B. Leznoff, *J. Am. Chem. Soc.* **2004**, *126*, 16117–16125.
[25] E. J. Fernández, J. M. Lopez-de-Luzuriaga, M. Monge, M. E. Olmos, R. C. Puelles, A. Laguna, A. A. Mohamed, J. P. Fackler, Jr., *Inorg. Chem.* **2008**, *47*, 8069–8076.
[26] A. Laguna, T. Lasanta, J. M. Lopez-de-Luzuriaga, M. Monge, P. Naumov, M. E. Olmos, *J. Am. Chem. Soc.* **2010**, *132*, 456–457.
[27] T. Abe, T. Suzuki, K. Shinozaki, *Inorg. Chem.* **2010**, *49*, 1794–1800.
[28] J. Pang, E. J.-P. Marcotte, C. Seward, R. S. Brown, S. Wang, *Angew. Chem.* **2001**, *113*, 4166–4169; *Angew. Chem. Int. Ed.* **2001**, *40*, 4042–4045.
[29] K. A. McGee, B. J. Marquardt, K. R. Mann, *Inorg. Chem.* **2008**, *47*, 9143–9145.
[30] W. Lu, M. C. W. Chan, K. K. Cheung, C. M. Che, *Organometallics* **2001**, *20*, 2477–2486.
[31] S. C. F. Kui, S. S.-Y. Chui, C.-M. Che, N. Zhu, *J. Am. Chem. Soc.* **2006**, *128*, 8297–8309.
[32] S. Das, P. K. Bharadwaj, *Inorg. Chem.* **2006**, *45*, 5257–5259.
[33] R. Pattacini, C. Giansante, P. Ceroni, M. Maestri, P. Braunstein, *Chem. Eur. J.* **2007**, *13*, 10117–10128.
[34] Z. Liu, Z. Bian, J. Bian, Z. Li, D. Nie, C. Huang, *Inorg. Chem.* **2008**, *47*, 8025–8030.
[35] C. A. Daws, C. L. Exstrom, J. R. Sowa, Jr., K. R. Mann, *Chem. Mater.* **1997**, *9*, 363–368.
[36] S. Kishi, M. Kato, *Mol. Cryst. Liq. Cryst. Sci. Technol., Sect. A* **2002**, *379*, 303–308.
[37] E. Cariati, X. Bu, P. C. Ford, *Chem. Mater.* **2000**, *12*, 3385–3391.
[38] A. L. Balch, *Angew. Chem.* **2009**, *121*, 2679–2682; *Angew. Chem. Int. Ed.* **2009**, *48*, 2641–2643.
[39] Z. Assefa, M. A. Omary, B. G. McBurnett, A. A. Mohamed, H. H. Patterson, R. J. Staples, J. P. Fackler, Jr., *Inorg. Chem.* **2002**, *41*, 6274–6280.
[40] V. J. Catalano, S. J. Horner, *Inorg. Chem.* **2003**, *42*, 8430–8438.
[41] Y. A. Lee, R. Eisenberg, *J. Am. Chem. Soc.* **2003**, *125*, 7778–7779.
[42] S. Mizukami, H. Houjou, K. Sugaya, E. Koyama, H. Tokuhisa, T. Sasaki, M. Kanesato, *Chem. Mater.* **2005**, *17*, 50–56.
[43] J. Schneider, Y. A. Lee, J. Perez, W. W. Brennessel, C. Flaschenriem, R. Eisenberg, *Inorg. Chem.* **2008**, *47*, 957–968.
[44] H. Ito, T. Saito, N. Oshima, N. Kitamura, S. Ishizaka, Y. Hinatsu, M. Wakeshima, M. Kato, K. Tsuge, M. Sawamura, *J. Am. Chem. Soc.* **2008**, *130*, 10044–10045.
[45] T. Abe, T. Itakura, N. Ikeda, K. Shinozaki, *Dalton Trans.* **2009**, 711–715.
[46] A. M. Kuchison, M. O. Wolf, B. O. Patrick, *Chem. Commun.* **2009**, 7387–7389.
[47] T. Tsukuda, M. Kawase, A. Dairiki, K. Matsumoto, T. Tsubomura, *Chem. Commun.* **2010**, *46*, 1905–1907.
[48] P. Pyykkö, *Angew. Chem.* **2004**, *116*, 4512–4557; *Angew. Chem. Int. Ed.* **2004**, *43*, 4412–4456.
[49] H. Schmidbaur, A. Schier, *Chem. Soc. Rev.* **2008**, *37*, 1931–1951.
[50] A. L. Balch, *Structure & Bonding* **2007**, *123*, 1–40.
[51] M. Osawa, I. Kawata, S. Igawa, A. Tsuboyama, D. Hashizume, M. Hoshino, *Eur. J. Inorg. Chem.* **2009**, 3708–3711.
[52] V. Pawlowski, H. Kunkely, C. Lennartz, K. Boehn, A. Vogler, *Eur. J. Inorg. Chem.* **2004**, 4242–4246.
[53] C. Kutal, *Coord. Chem. Rev.* **1990**, *99*, 213–252.
[54] A. Vogler, H. Kunkely, *Coord. Chem. Rev.* **2002**, *230*, 243–251.
[55] M. Nishio, *CrystEngComm* **2004**, *6*, 130–158.
[56] L. Lo Presti, R. Soave, R. Destro, *J. Phys. Chem. B* **2006**, *110*, 6405–6414.
[57] H. P. Zhou, P. Wang, F. Y. Hao, H. P. Ye, Q. Zhao, R. L. Zhang, Y. P. Tian, J. Y. Wu, X. T. Tao, M. H. Jiang, *J. Mol. Struct.* **2008**, *892*, 316–319.
[58] F. Grepioni, G. Cojazzi, S. M. Draper, N. Scully, D. Beraga, *Organometallics* **1998**, *17*, 296–307.
[59] V. R. Thalladi, H. C. Weiss, D. Bläser, R. Boese, A. Nangia, G. R. Desiraju, *J. Am. Chem. Soc.* **1998**, *120*, 8702–8710.
[60] K. Reichenbächer, H. I. Süss, J. Hulliger, *Chem. Soc. Rev.* **2005**, *34*, 22–30.
[61] T. M. McCleskey, H. B. Gray, *Inorg. Chem.* **1992**, *31*, 1733–1734.
[62] V. W. W. Yam, C. L. Chan, S. W.-K. Choi, K. M.-C. Wong, E. C.-C. Cheng, S.-C. Yu, P.-K. Ng, W.-K. Chan, K.-K. Cheung, *Chem. Commun.* **2000**, 53–54.
[63] C. D. Delfs, H. J. Kitto, R. Stranger, G. F. Swiegers, S. B. Wild, A. C. Willis, G. J. Wilson, *Inorg. Chem.* **2003**, *42*, 4469–4478.
[64] A. Pintado-Alba, H. de La Riva, M. Nieuwhuyzen, D. Bautista, P. R. Raithby, H. A. Sparkes, S. J. Teat, J. M. López-de-Luzuriaga, M. C. Lagunas, *Dalton Trans.* **2004**, 3459–3467.
[65] K. Saito, T. Tsukuda, K. Matsumoto, T. Tsubomura, *Bull. Chem. Soc. Jpn.* **2007**, *80*, 533–535.
[66] M. Ferrer, A. Gutiérrez, L. Rodríguez, O. Rossell, J. C. Lima, M. Font-Bardia, X. Solans, *Eur. J. Inorg. Chem.* **2008**, 2899–2909.
[67] A. Kobayashi, T. Yonemura, M. Kato, *Eur. J. Inorg. Chem.* **2010**, 2465–2470.
[68] N. Mézailles, L. Ricard and F. Gagosz, *Org. Lett.* **2005**, *7*, 4133–4136.

[69] T. Higashi, *Program for absorption correction*, Rigaku Corp., Tokyo, Japan, **1995**.
[70] M. C. Burla, R. Caliandro, M. Camalli, B. Carrozzini, G. L. Cascarano, L. De Caro, C. Giacovazzo, G. Polidori, R. Spagna, *J. Appl. Cryst.* **2005**, *38*, 381–388.
[71] M. Hoshino, H. Sonoki, Y. Miyazaki, Y. Iimura and K. Yamamoto, *Inorg. Chem.* **2000**, *39*, 4850–4857.
[72] R. G. Parr, W. Yang, *Density-functional Theory of Atoms and Molecules*, Oxford University Press, Oxford, **1994**.
[73] Gaussian 03, Revision D.01, M. J. Frisch, G. W. Trucks, H. B. Schlegel, G. E. Scuseria, M. A. Robb, J. R. Cheeseman, J. A. Montgomery, Jr., T. Vreven, K. N. Kudin, J. C. Burant, J. M. Millam, S. S. Iyengar, J. Tomasi, V. Barone, B. Mennucci, M. Cossi, G. Scalmani, N. Rega, G. A. Petersson, H. Nakatsuji, M. Hada, M. Ehara, K. Toyota, R. Fukuda, J. Hasegawa, M. Ishida, T. Nakajima, Y. Honda, O. Kitao, H. Nakai, M. Klene, X. Li, J. E. Knox, H. P. Hratchian, J. B. Cross, V. Bakken, C. Adamo, J. Jaramillo, R. Gomperts, R. E. Stratmann, O. Yazyev, A. J. Austin, R. Cammi, C. Pomelli, J. W. Ochterski, P. Y. Ayala, K. Morokuma, G. A. Voth, P. Salvador, J. J. Dannenberg, V. G. Zakrzewski, S. Dapprich, A. D. Daniels, M. C. Strain, O. Farkas, D. K. Malick, A. D. Rabuck, K. Raghavachari, J. B. Foresman, J. V. Ortiz, Q. Cui, A. G. Baboul, S. Clifford, J. Cioslowski, B. B. Stefanov, G. Liu, A. Liashenko, P. Piskorz, I. Komaromi, R. L. Martin, D. J. Fox, T. Keith, M. A. Al-Laham, C. Y. Peng, A. Nanayakkara, M. Challacombe, P. M. W. Gill, B. Johnson, W. Chen, M. W. Wong, C. Gonzalez, and J. A. Pople, Gaussian, Inc., Wallingford CT, **2004**.
[74] C. Lee, W. Yang, R. G. Parr, *Phys. Rev. B* **1988**, *37*, 785–789.
[75] A. D. Becke, *J. Chem. Phys.* **1993**, *98*, 5648–5652.
[76] P. J. Hay, W. R. Wadt, *J. Chem. Phys.* **1985**, *82*, 270–283.
[77] P. Pyykkö, F. Mendizabal, *Inorg. Chem.* **1998**, *37*, 3018–3025.
[78] M. Couty, M. B. Hall, *J. Comput. Chem.* **1996**, *17*, 1359–1370.
[79] K. Barakat, T. R. Cundari, *Chem. Phys.* **2005**, *311*, 3–11.
[80] R. L. Martin, *J. Chem. Phys.* **2003**, *118*, 4775–4777.
[81] K. Nozaki, *J. Chin. Chem. Soc.* **2006**, *53*, 101–112.
[82] J. E. Carpenter, F. Weinhold, *THEOCHEM* **1988**, *169*, 41–62.

Received: July 6, 2010
Published online: September 30, 2010

